IEEE Access
Multidisciplinary | Rapid Review | Open Access Journal

IEEE ENGINEERING IN MEDICINE AND BIOLOGY SOCIETY SECTION

Received September 30, 2021, accepted October 13, 2021, date of publication October 15, 2021, date of current version October 26, 2021.

Digital Object Identifier 10.1109/ACCESS.2021.3120717

Screening of COVID-19 Suspected Subjects Using Multi-Crossover Genetic Algorithm Based Dense Convolutional Neural Network

DILBAG SINGH[1], (Member, IEEE), VIJAY KUMAR[2], MANJIT KAUR[3], (Member, IEEE), MOHAMED YASEEN JABARULLA[1], AND HEUNG-NO LEE[1], (Senior Member, IEEE)

[1]School of Electrical Engineering and Computer Science, Gwangju Institute of Science and Technology (GIST), Gwangju 61005, South Korea
[2]Department of Computer Science and Engineering, National Institute of Technology Hamirpur, Hamirpur 177005, India
[3]School of Engineering and Applied Sciences, Bennett University, Greater Noida 201310, India

Corresponding author: Heung-No Lee (heungno@gist.ac.kr)

This work was supported in part by the National Research Foundation of Korea (NRF) funded by the Government of Korea (MSIP) under Grant NRF-2021R1A2B5B03002118.

ABSTRACT Fast and accurate screening of novel coronavirus (COVID-19) suspected subjects plays a vital role in timely quarantine and medical care. Deep transfer learning-based screening models on chest X-ray (CXR) are effective for countering the COVID-19 outbreak. However, an efficient screening of COVID-19 is still a huge task due to the spatial complexity of CXRs. In this paper, a dense convolutional neural network (DCov-Net) based transfer learning model is proposed for the screening of COVID-19 suspected subjects using CXR images. A modified multi-crossover genetic algorithm (MMCGA) is then proposed to tune the hyper-parameters of DCov-Net. Majority of the existing COVID-19 diagnosis models are not interpretable as they do not provide any transparency to the users. Therefore, the concept of heat-maps is used to achieve explainability and interpretability. MMCGA based DCov-Net is implemented on a multiclass dataset that contains four different classes. Experimental results reveal that MMCGA based DCov-Net achieves better performance than the existing models. The proposed MMCGA based DCov-Net can be utilized for initial screening of COVID-19 suspected subjects with an accuracy of 99.34 ± 0.51 %.

INDEX TERMS COVID-19, diagnosis, chest-CT, ensemble, deep learning.

I. INTRODUCTION

Since December 2019, the entire world has been experiencing the epidemic of a novel coronavirus (COVID-19). It is due to severe acute respiratory syndrome coronavirus 2 (SARS-CoV-2) [1], [2]. The laboratory examinations of COVID-19 patients have elevated lactate dehydrogenase, reduced lymphocyte count, reduced or normal leukocyte count, elevated myoglobin, and elevated creatine kinase [3], [4]. The lesser lymphocyte count is found in severe cases. In some cases, the patients have a severe provocative storms that can cause death [5]. Therefore, the early screening of COVID-19 suspected subjects is desirable to decrease the mortality rate and ensure an efficient treatment of patients. For this, chest X-ray (CXR) images are utilized to monitor the common symptoms found in infected patients.

The associate editor coordinating the review of this manuscript and approving it for publication was Chulhong Kim.

For efficient screening of COVID-19 suspected subjects, the reverse transcription polymerase chain reaction (RT-PCR) is utilized as a standard approach [6]. Due to time-consuming and strict testing conditions of RT-PCR kit, fast and early testing of suspected subjects is limited. Moreover, RT-PCR kits suffer from high false-negative rates [7].

Recently, deep learning models are widely utilized by researchers for diagnosis of COVID-19 suspected subjects from radiological images. The deep learning-based localization and classification models have been designed for marking COVID-19 infected areas in ultrasound images [6]. Automated classification of COVID-19 suspected subjects from CT was developed by designing an deep 3D learning model. This model semantically produces deep-3D occurrences following the probably infected region in chest CT images to screen the COVID-19 suspected subjects [8]. A patch-based convolutional neural network (CNN) model was proposed for screening of COVID-19 by

using CXRs. The patch-based CNN model used a significantly few trainable variables for COVID-19 screening [9].

COVID-19 screening and lesion localization can be achieved by using weakly supervised model from chest CT images. A pretrained UNet model was implemented for lung region segmentation. Thereafter, 3D-CNN was used to recognize COVID-19 suspected subjects [10]. More discriminative diagnosis of COVID-19 suspected subjects from CT Images can be achieved using prior attention residual learning [11].

An infection segmentation deep network (Inf-net) based COVID-19 Infected lung segmentation approach was implemented in [12] for chest CT images. To improve the learning ability, a semisupervised segmentation framework was also utilized. A COVID-19 pneumonia lesion segmentation (COPLE-Net) model was presented in [13] for pneumonia lesion segmentation from chest computed tomography (CT) images.

However, the existing COVID-19 screening models suffer from underfitting issues due to the lack of labeled datasets. Additionally, the existing models have focused on COVID-19 screening as a binary or three-class problem. However, it is found that there exists a similarity between CXRs of COVID-19 suspected subjects and CXRs of patients who have other lung diseases.

CT screening in the initial patient indicates significant sensitivity as compared with RT-PCR [14]. Also, it has been found that when COVID-19 infection is very low in patients (i.e., an early stage of infection), CT-based diagnosis shows significantly more sensitivity as compared to RT-PCR [15]. Due to the high increase in COVID-19 suspected subjects every day, the routine utilization of CT spots put a massive burden on radiologists and possible infection of CT suite hence, many researchers have started using CXR images for initial screening of COVID-suspected subjects [9], [16].

Therefore, the development of a fast and efficient automated COVID-19 screening model from CXR images is still a challenging issue. Compared with the competitive models, the proposed DCov-Net has the following advantages:

1) A dense convolutional neural network (DCov-Net) based transfer learning model is proposed for the screening of COVID-19 suspected subjects using CXR images.
2) Modified multi-crossover genetic algorithm (MMCGA) is proposed to tune the hyper-parameters of DCov-Net.
3) The concept of heat-maps is also used to achieve explainability and interpretability.
4) Data augmentation is utilized to augment the size of the dataset.
5) The proposed MMCGA based DCov-Net is implemented on a multiclass dataset that contains four classes.

The remaining structure of this paper is as follows: The related work is presented in Section II. Section III describes the proposed DenseNet based model. Section IV presents the experimental results and discussion Section V concludes the paper.

II. RELATED WORK

Deep learning models have been extensively utilized in the area of biomedical imaging [17], [18]. These approaches can be used in detecting abnormalities from CXR and CT scan [19], [20]. Due to low ionizing radiation exposure to patients, CXR is preferred over CT scans [21]. Das *et al.* [22] proposed a pretrained transfer learning architecture for diagnosis of COVID-19 suspected cases. The weights were fine-tuned through a pretrained Xception network. It has achieved 97.41% accuracy. Mahmud *et al.* [23] implemented a deep learning model namely CovXNet, for the screening of COVID-19 suspected subjects from CXRs. Depthwise dilated convolution was used for the extraction of diverse features from CXR. These extracted features were applied to gradient-based discriminative localization to discriminate abnormal regions in CXR. Their model attained an accuracy of 97.40%. Singh *et al.* [24] designed a differential evolution-based CNN (DCNN) for diagnosis of coronavirus infections using CXR. The hyper-parameters of CNN were tuned through multiobjective adaptive differential evolution (MADE). It has attained an overall classification accuracy of 94.48%. Togacar *et al.* [25] used the fuzzy based preprocessing approach for CXR. The preprocessed images are structured using the stacking approach. The efficient features were extracted through MobileNet and SqueezeNet models. A support vector machine (SVM) was then utilized to build the screening model from the extracted features. Their model attained an accuracy of 98.25% on 1357 CXR images.

Behzadi-Khormouji *et al.* [26] proposed a ChestNet model for detecting consolidation using CXR. ChestNet used a lesser number of max-pooling layers compared with VGG16 and DenseNet121. The accuracy obtained from their approach was 94.67%. Altan and Karasu [27] developed a hybrid model that consists of curvelet transformation, deep learning, and the chaotic salp algorithm for distinguishing COVID-19 imaging patterns from CXR images. The curvelet transformation was applied on a CXR for extracting coefficients. Chaotic salp swarm algorithm (CSA) was used to optimize the extracted coefficients. These optimized coefficients were applied to the EfficentNet-B0 model for screening of COVID-19. Their model was tested on 1596 CXR images. This model has shown 99% accuracy for screening of COVID-19 suspected subjects. Rahimzadeh and Attar [28] hybridized Xception and ResNet50V2 for the screening of COVID-19 from CXRs. 11302 CXRs were used to validate the performance of the hybrid model. The average accuracy obtained from the hybrid model was 91.40%. Ucar and Korkmaz [29] proposed a deep Bayes-SqueezeNet based COVIDiagnosis-Net for diagnosis of coronavirus infected persons. COVIDiagnosis-Net achieved 98.30% accuracy. Tuncer *et al.* [30] designed a screening model for COVID-19 using CXR images.

They used grayscale conversion approach for preprocessing of CXRs. Residual exemplar local binary pattern (ResExLBP) was used for feature iteration. These characteristics were utilized in a SVM to distinguish COVID-19 from healthy subjects. It has attained 99.29% accuracy. However, a limited number of chest images were used for validation purposes. Alqudah *et al.* [31] employed artificial intelligence approaches for the identification of coronavirus infection in patients using CXR. The imaging features were extracted using CNN. SVM was then used for building COVID-19 screening model. This SVM based model has achieved 95.20% accuracy. Hemdan *et al.* [32] utilized seven different CNN architectures and implemented COVIDX-Net model for screening of COVID-19 from CXR images. VGG19 and DenseNet201 attained 90% accuracy using fifty CXRs. Wang *et al.* [33] developed a deep learning model namely COVID-Net for the diagnosis of COVID-19 from CXR. COVID-Net was trained using over 13975 CXR images. COVID-Net has shown the accuracy of 93.3%. It is observed from the literature review that there is scope for improvement in deep learning models for screening of COVID-19 suspected persons.

Yamac *et al.* [34] utilized a convolution support estimation network (CSEN) for COVID-19 diagnosis. CSEN utilized a noniterative mapping from query to ideally sparse representation coefficient support. Thus, it can handle critical information for class decision in representation-based approaches. CSEN has shown 98% sensitivity and 95% specificity to diagnose COVID-19 suspected cases. Abbas *et al.* [35] designed a self-supervised super sample decomposition for transfer learning (4S-DT) model. The super sample decomposition of unlabeled CXRs was utilized to form self-supervised learning model. It has shown an accuracy of 99.8% and 97.54% on two different datasets. Ismael and Sengur [36] designed a transfer learning based SVM (TL-SVM) model. TL-SVM has utilized various transfer learning models to extract the features from CXRs. The extracted features were classified using SVM. It has shown the accuracy of 94.7%. Hasan [37] has designed a hybrid two-dimensional empirical mode decomposition (2DEMD) based CNN (HT-CNN) model to diagnose COVID-19 suspected cases. Intrinsic mode functions were generated using 2DEMD. CNN model was utilized to diagnose COVID-19 suspected cases. It has shown the accuracy of 99.01%. Hasan *et al.* [38] proposed DenseNet-121 CNN model. Data augmentation was used to augment the dataset. It has shown the accuracy of 92% on CT images dataset. Sarker *et al.* [39] designed an explainability based COVID-DenseNet model. Transfer learning was used by utilizing the pre-trained CheXNet model. It has achieved an accuracy of 96.49% and 93.71%, for two-class and three-class datasets, respectively. Misra *et al.* [40] designed an ensemble based multi-channel pre-trained ResNet (MC-ResNet) for CXRs. Three ResNet based variants were used to build MC-ResNet. It has achieved an accuracy of 95.5% and 93.9% for raw and refined datasets, respectively.

It is clear from the literature that the development of early stage recognition of COVID-19 suspected subjects is an open area of research. In particular, the use of a deep transfer learning model can be explored further to improve the sensitivity and specificity of automated screening tools. The existing automated screening models are sensitives to their initial hyper-parameters. Majority of the existing COVID-19 diagnosis models are not interpretable as they do not provide any transparency to the users. Additionally, an efficient automated screening model can distinguish among the other kinds of lung diseases such as pneumonia and lung opacity.

III. PROPOSED MODEL

This section provides the mathematical formulation of the proposed DCov-Net-based screening of COVID-19 suspected subjects. Initially, the labeled dataset is obtained and then the dataset is decomposed into three sets for training, testing, and validation. As the obtained dataset is small in size, data augmentation is used. Thereafter, DCov-Net is proposed. The initial parameters of DCov-Net are then tuned using MMCGA. Finally, MMCGA based DCoV-Net is build to recognize the suspected patient as infected (i.e., COVID-19 (+ve) or pneumonia or lung opacity) or as a healthy person.

A. COVID-19 SCREENING MODEL

The primary objective is to design a model that can automatically screen COVID-19 suspected subjects from their respective CXRs. Figure 1 presents the block diagram of DCov-Net based COVID-19 screening model. Initially, ImageNet [41] dataset is used to obtain the transferable coefficients from DenseNet model. Thereafter, data augmentation is applied to the obtained dataset. Fine-tuning of DenseNet is then achieved using the training dataset with a pretrained DenseNet model. The trained DenseNet based COVID-19 screening model can successfully classify a suspected person as infected (i.e., COVID-19 (+ve), pneumonia or lung opacity) or as a healthy person.

B. DenseNet MODEL

In this paper, a pretrained DenseNet model is utilized. Figure 2 demonstrates the diagrammatic flow of DenseNet-based COVID-19 screening model. It contains three transition blocks (*TB*) and four dense blocks (*DB*), respectively. In Fig. 2, F_i shows a composite function of three operators such as B_N, $FReLU$, and C_V. X_i represents the computed feature map by i^{th} layer. Also, $i = 1, 2, 3, \ldots, I$. I shows number of layers. Like ResNet [42], DenseNet considers dense links to enhance the relationship between perspective information. The input of every layer includes the input and output of the preceding layer. Thus, it improves the information transmission to reuse the features efficiently. Features of CXRs are dense and redundant in nature. Combined with the constrained dataset, neural network-based model building is susceptible to gradient loss. Therefore, the trained model suffers from the overfitting issue. DenseNet integrates the

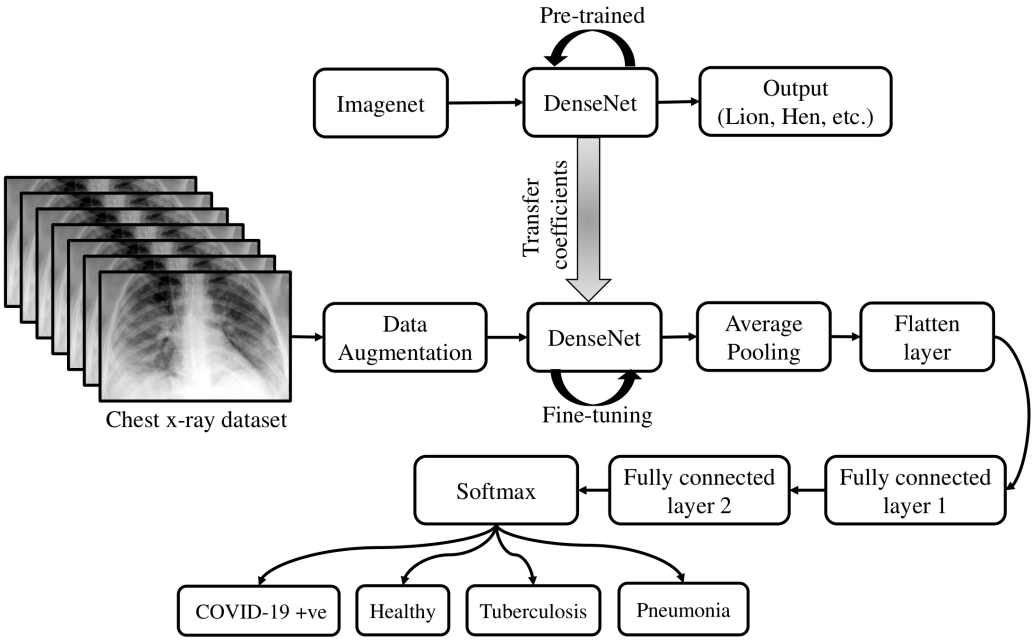

FIGURE 1. Proposed DCov-Net-based COVID-19 screening model.

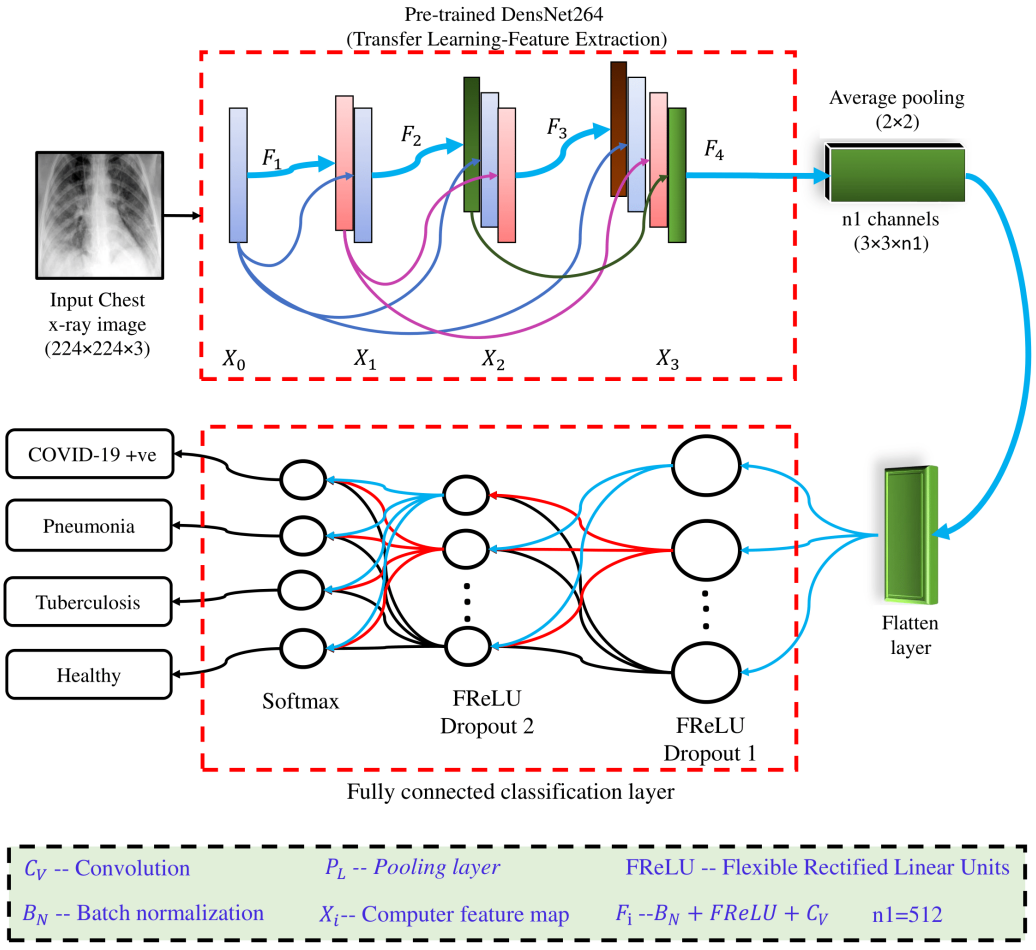

FIGURE 2. Architecture of DenseNet264-based automated screening model for COVID-19 suspected subjects.

feature map to overcome this gradient loss issue. Thus, it can efficiently be obtained the potential features from CXRs.

Although, there exist some similarities in the modules of DenseNet and ResNet but there are considerable variations in these modules. It is found that the skip connection of ResNet's residual module can easily aggregate x_{l-1} and the nonlinear transformation of x_{l-1} as:

$$x_l = F(x_{l-1}) + x_{l-1} \tag{1}$$

Here, x_l denotes the output of layer l and $F(\bullet)$ defines a nonlinear transformation. Thus, the model can adapt the input's residual mapping to overcome the gradient loss issue.

Dense block (DB) module concatenates the feature map's connection instead of summation as:

$$x_l = F([x_0, x_1, \ldots, x_{l-1}]) \tag{2}$$

At i^{th} layer, there are $K \times (i-1) + K_0$ convolution maps. K defines convoluted feature maps for every layer. In DenseNet, the input of every layer contains the feature maps of all preceding layers (see Figure 9). DenseNet develops a L layer architecture with $\frac{L(L+1)}{2}$ connections.

In this paper, DenseNet264 is used. In the dense block (*DB*), both contain different numbers of convolution layers. Table 1 depicts the characteristics of both models.

C. TRANSFER LEARNING

Transfer learning is generally used for fine-tuning deep learning models to prevent local optimization issues. Instead of model initialization with random weights, it acts as an initial point of the new model [43]. Thus, it helps in the fast building of a new deep learning model with significant results even for small size datasets.

In fully connected layer, every neuron is associated with every neuron of the preceding layer. As the input of preceding layer is $2D$ feature map, therefore, Bernoulli function is utilized. It randomly computes a vector t^{l-1} following the [0, 1] distribution with a specific probability (p). It can be computed as [44]:

$$t^{l-1} = Bernoulli(p) \tag{3}$$
$$x^{l-1} = t^{l-1} \times c^{l-1} \tag{4}$$
$$x^{l} = f(w^k \times x^{l-1} + o^l) \tag{5}$$

Here, the vector dimension is c^{l-1}. k shows feature maps. o^1 and w^1 indicate the offset and weighting variables of the fully connected layer, respectively. Dropout is also used to prevent overfitting issue. Dropout blocks some neurons with specific probability on random basis. The computed feature map is then weighted and added to the bias offset. Thereafter, softmax activation function is used.

D. ACTIVATION AND LOSS FUNCTION

In this work, the softmax activation function is used at the output layer of the proposed DCov-Net for multiclass classification. The softmax function ($P(c, s)$) can be defined as:

$$P(c, s) = \frac{P(s, c) \times P(c)}{\sum_{n=1}^{C} P(n) \times P(s, n)} \tag{6}$$

Here, c defines the total number of classes, $P(c)$ and $P(s, c)$ denote the class probability and conditional probability, respectively. s shows the probability of a sample that belongs to c class. $P(c, s)$ can be rewritten as:

$$P(c, s) = \frac{exp(\beta^c[s])}{\sum_{n=1}^{C} exp(\beta^n[s])} \tag{7}$$

where

$$\beta^c = ln[P(s, c) \times P(c)] \tag{8}$$

The binary cross entropy is utilized as a loss function. It can be evaluated as:

$$loss = -\sum_{i=1}^{n} \hat{y}_i \log y_i + (1 - \hat{y}_i) \log(1 - y_i) \tag{9}$$

Here, n shows the number of test CXRs and y_i represents the output of the deep learning model. *loss* approaches 0, when y_i approaches $\hat{y}_i$. $\hat{y}_i$ defines the accurate value of the desired output.

TABLE 1. Architectures of proposed MMCGA based DCov-Net model with stride=2.

Block	Output size	Size
Convolution	112×112	$7 \times 7\ C_v$
Pooling	56×56	3×3 max pool
Dense Block1	56×56	$\begin{bmatrix} 1 \times 1\ C_v \\ 3 \times 3\ C_v \end{bmatrix} \times 6$
Transition Layer1	$\begin{bmatrix} 56 \times 56 \\ 28 \times 28 \end{bmatrix}$	$\begin{bmatrix} 1 \times 1\ C_v \\ 2 \times 2\ average\ pool \end{bmatrix}$
Dense Block2	28×28	$\begin{bmatrix} 1 \times 1\ C_v \\ 3 \times 3\ C_v \end{bmatrix} \times 12$
Transition Layer2	$\begin{bmatrix} 28 \times 28 \\ 14 \times 14 \end{bmatrix}$	$\begin{bmatrix} 1 \times 1\ C_v \\ 2 \times 2\ average\ pool \end{bmatrix}$
Dense Block3	14×14	$\begin{bmatrix} 1 \times 1C_v \\ 3 \times 3C_v \end{bmatrix} \times 64$
Transition Layer3	$\begin{bmatrix} 14 \times 14 \\ 7 \times 7 \end{bmatrix}$	$\begin{bmatrix} 1 \times 1\ C_v \\ 2 \times 2\ average\ pool \end{bmatrix}$
Dense Block4	7×7	$\begin{bmatrix} 1 \times 1C_v \\ 3 \times 3C_v \end{bmatrix} \times 48$
Average Pooling	2×2	$3 \times 3 \times n1$
Flatten Layer	[None, $n1$]	$1 \times n1$
Flatten Layer	[None, $n1$]	$1 \times n1$
Fully connected layer1 (Dense)	[None, Tuned*]	[None, Tuned*]
Fully connected layer2 (Dense)	[None, Tuned*]	[None, Tuned*]
Softmax	[None, 4]	[None, 4]

* Obtained from MMCGA

E. OPTIMIZATION OF HYPER-PARAMETERS

Proposed DenseNet model is sensitive to its initial parameters. Therefore, it is required to tune the hyper-parameters of DenseNet to achieve the efficient results. Table 2 depicts the search space for hyper-parameters of the proposed DenseNet model.

TABLE 2. Search space for hyper-parameters of the proposed DenseNet.

Attribute	Range
Decay rate	[0, 1]
Learning rate	[0.1, 0.01, 0.001]
Fully connected layer 1	[50, 200]
Fully connected layer 2	[50, 200]
Dropout 1	[0.1, 0.5]
Dropout 2	[0.1, 0.5]

In genetic algorithm, new solutions are searched using crossover operator and it also influence the optimization results. Therefore, many crossover operators are proposed in the literature to efficiently form the new solutions. However, the selection of the efficient crossover operator according to the problem is an open area of research. To resolve this issue, Xue *et al.* [45] has designed a multi-crossover genetic algorithm (MCGA). Five crossover operators were used to form the new solutions for next iteration. According to their performance during evolution process, a probability was assigned to each of them. Based on their probabilities crossover operator was selected using roulette wheel selection during the evolution process.

In this paper, a modified MCGA (MMCGA) is proposed to reduce the complexity and increase the computational speed. In MMCGA, three crossover operators are used that will be adaptively selected during evolution step. Also, elitist non-dominated sorting [46] is used to evaluate the best solution for DCoV-Net. The step by step approach is discussed in Algorithm 1.

iPop (): Initially, population P is composed by randomly generating N solutions based upon their range values as reported in Table 2. **iACS:** Adaptive crossover selection function (ACS) and its associated parameters are also imitated. Initially, the probability of every crossover operator is $1/Q$. Q indicates available crossovers used in MMCGA. **iRWS():** Roulette wheel selection is used to select one crossover operator depending upon their respective probability values computed from ACS. **iCros():** Depending upon ACS values (a_v), a specific crossover operator is then applied to obtain child solutions. Two parents are randomly selected. **iMut():** Uniform mutation operator is also used to form new solutions. All new solutions are then stored in offspring population(P_δ). **iCred():** Dominance relationship is then computed between parents and children and corresponding performance is stored in nR and nP. During $N/2^{th}$ step, P_δ is evaluated. **iSel():** Elitist non-dominated sorting [46] and crowded distance [47] techniques are then utilized to select N individuals from R ($P \cup P_\delta$). **iDomin():** dominance comparison is utilized to assign the reward or penalty to the selected parent and child solutions.

The reward and penalty of solutions in given step is stored in two matrices $RW_{TH\times Q}$ and $PL_{TH\times Q}$, respectively. After every TH number of steps, ACS will be updated using $RW_{TH\times Q}$ and $PL_{TH\times Q}$. The evolution process keep repeating until the fitness evaluations do not exceed F_e (refer [45]).

Algorithm 1 MMCGA Based DCoV-Net

Input: Maximum fitness evaluations (F_e), Population size (N), Number of crossover operators (Q), and ACS iterative threshold (TH).

Output: Tuned parameters for DCov-Net

```
P ← iPop(N)
Initialize nR, nP, RW_{TH×Q}, and PL_{TH×Q}.
P̂ = p_1, p_2, ..., p_Q ← iACS(Q)
k ← 0
nFE ← 0
P_δ ← φ
while nFE < F_e do
  for i = 1toN/2 do
    a_v ← iRWS (P̂)
    Randomly select two individuals as parents: P_p
    P_c ← iCros(P_p, a_v)
    P_c ← iMut(P_c )
    nFE ← nFE + 2
    [nR, nP] ← iCred(P_p, P_c)
    Add P_c to P_δ
  end for
  k ← k + 1
  Append nR to k^th row of RW_{TH×Q}
  Append nP to k^th row of PL_{TH×Q}
  if k = TH then
    P̂ ← iACS( RW_{TH×Q}, PL_{TH×Q} )
    k = 0
  end if
  R ← P ∪ P_δ
  P ← iSel(R)
  Select non-dominated solutions in P as T_P
  Tuned parameters ← T_P
end while
return Optimal parameters
```

The steps of proposed MMCGA are discussed in the succeeding subsections.

1) MULTI-OBJECTIVE FITNESS FUNCTION

The main objective of MMCGA is to obtain an optimal set of hyper-parameters with maximum performance in terms of sensitivity and specificity. Thus, multi-objective fitness function can be computed as:

$$\max F(X) = \{f_1(X) \text{ and } f_2(X)\} \tag{10}$$

where X is a solution. f_1 and f_2 computes the sensitivity and specificity values, respectively. These are used to obtain optimal hyper-parameter (X) of DCoV-Net

Algorithm 2 Credit Card Assignment (iCred ())

Input: Parents (P), Children (R), iACS based crossover (q)
Output: nR, nP $[n_d, d_s] \leftarrow$ iDomin(P) //n_d and d_s refer to the sets of non-dominated and dominated solutions, respectively.

```
if d_s ≠ φ then
    // Dominated parent, and suppose P_1 ≺ P_2.
    for i = 1 to 2 do
        if P_1 ≺ R_i then
            nP_q ← nP_q + 1
        else
            nR_q ← nRnR_q + 1
        end if
    end for
else
    // Non-dominated parent.
    for i = 1 to 2 do
        if P_1 ⊀ R_i P_2 ⊀ R_i then
            nR_q ← nRnR_q + 1
        else
            nP_q ← nP_q + 1
        end if
    end for
end if
P ← iPop (N)
return Tuned parameters for DCov-Net
```

2) CROSSOVER OPERATORS

In this paper, three well-known crossover operators namely single-point [47], Reduced surrogate [48], [49], and chaotic crossover operator [50] have been selected. Single-point [47] is selected as it is the most efficient operator concerning the computational effort [45].

Reduced surrogate [48], [49] crossover operator is selected because it avoids the unwanted crossover operations in case of the parents having same genes. This operator initially checks for the individual genes in the parents. It forms a set of possible crossover points where the genes of both parents are different. If there is no such crossover point then no action will be taken. The chaotic crossover operator [50] helps to form well-distributed and well-converged set of Pareto-optimal solutions.

3) REWARD AND PENALTY

Rewards and penalties are assigned to the solutions by defining two vectors (i.e., nR and nP) as:

$$nR = [000]_{1\times Q} \tag{11}$$

$$nP = [000]_{1\times Q} \tag{12}$$

Pareto dominance among the solutions is utilized to update nR and nP.

a: DOMINATED PARENT

Assume that parent 1 (P_1) is dominated by P_2, then the pareto dominance relationship of every child solution is compared with P_2. If the child solution is not dominated by P_2, then set $nR_q + 1$. Otherwise set $nP_q + 1$.

b: NON-DOMINATED PARENT

Every child solution's pareto dominance is compared with its both parents. If it is not dominated by both parents, then set $nR_q + 1$, otherwise set $nP_q + 1$. Algorithm 2 shows the step by step updation of reward and penalty values (refer [45]).

4) UPDATION OF ACS

ACS is used to update the selection probability of every crossover operator. It is updated after every TH iterations (for more details [51]). Two matrices, $RW_{TH\times Q}$ and $PL_{TH\times Q}$, are utilized to store nR and nP values, respectively, by rows till TH iterations. Recent TH's n_R and nP values are used to update ACS. To compute the probability for q^{th} ($q = 1, 2, \ldots, Q$) operator, summation of q^{th} column of RW and PL is performed, respectively:

$$S_q^1 = \sum_{k=1}^{TH} RW_{k,q} \tag{13}$$

$$S_q^2 = \sum_{k=1}^{TH} PL_{k,q} \tag{14}$$

Here, S_q^1 shows numbers of promising solutions obtained by using the q^{th} crossover during last TH iterations. S_q^2 shows the non-promising solutions. ACS for q^{th} crossover can be evaluated as:

$$S_q^3 = \begin{cases} \delta, & \text{if } S_q^1 = 0, \\ if S_q^1 = 0, & \text{otherwise.} \end{cases} \tag{15}$$

$$S_q^4 = \frac{S_q^1}{S_q^3 + S_q^2} \tag{16}$$

Here, $\delta = 0.0001$ is a small number used to prevent being divided by 0 if the q^{th} crossover is never selected during last TH iterations.

Also, S_q^4 is the probability allocated to q^{th} crossover. To normalize the probabilities of each crossover, normalization is achieved as:

$$p_q = \frac{S_q^4}{\sum_{q=1}^{Q} S_q^4} \tag{17}$$

Here, p_q shows the normalized probability for q^{th} crossover.

Table 3 shows tuned hyper-parameters obtained from optimization algorithm.

Figure 3 shows the training and validation analysis of the proposed model without using MMCGA. The proposed model has been tested by considering various hyper-parameters on trial and error basis. We have selected those hyper-parameters which have achieved better performance as compared among all the trial and error basis based hyper-parameters. It has shown the testing accuracy of 98.48% when number of iterations are set to be 580.

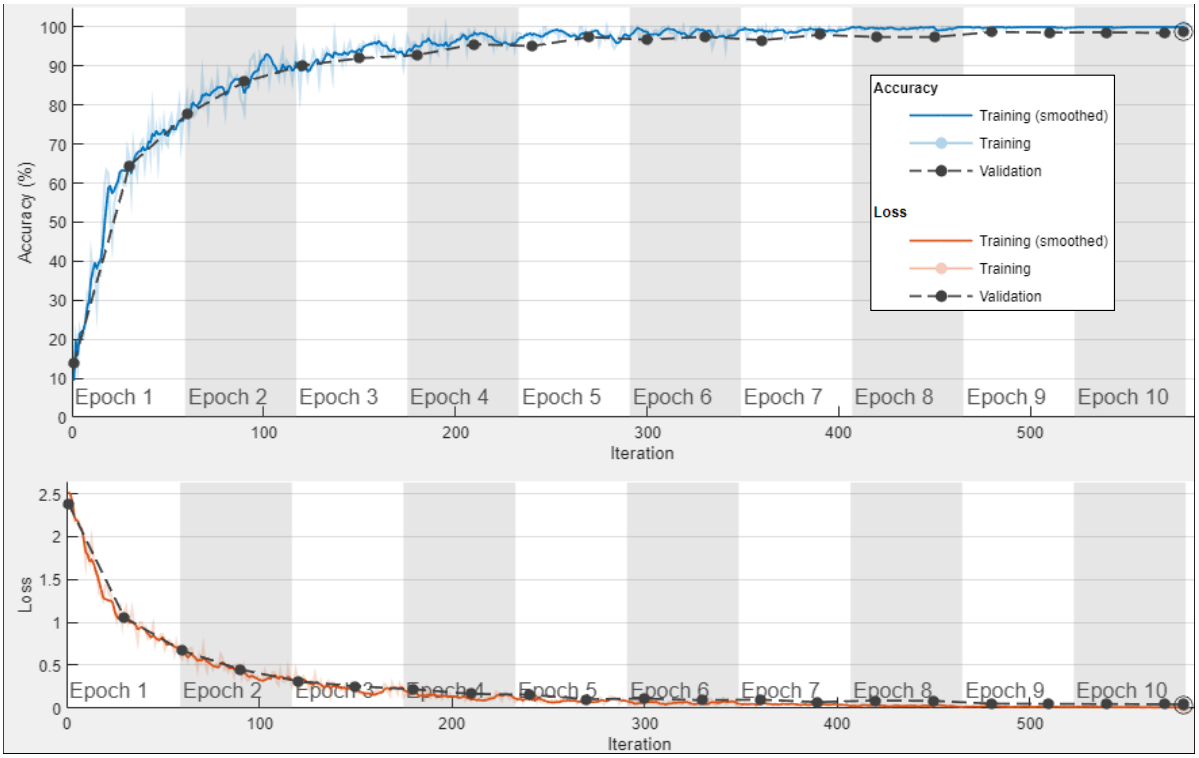

FIGURE 3. Training and validation analysis of the proposed model without using MMCGA.

TABLE 3. Obtained optimized hyper-parameters of the proposed DenseNet.

Attribute	Range
Decay rate	0.65
Learning rate	0.1
Fully connected layer 1	68
Fully connected layer 2	114
Dropout 1	0.27
Dropout 2	0.22

The proposed DCov-Net model is then trained on the optimized parameters obtained from MMGCA (see Table 3). In Figure 4, training and validation analysis of MMGCA based proposed model is presented. It has achieved the testing accuracy of 99.81% when number of iterations are set to be 580. Therefore, from Figures 3 and 4, it is observed that the optimized hyper-parameters based proposed model has achieved better performance with good convergence speed. MMCGA based DCoV-Net has shown an average improvement of 1.33% as compared to the accuracy obtained from trial and error basis based DCoV-Net.

IV. EXPERIMENTAL RESULTS

MMCGA based DCov-Net is tested on four-class CXR dataset. The performance of MMCGA based DCov-Net is compared with various competitive models such as CNN [9], AlexNet [52], VGGNet [26], Inceptionnet-v1 [53], ResNet [28], Inceptionnet-v3 [53], DenseNet [26], Xception [28], Inception-ResNet [54], Inceptionnet-V4 [53], and ResNeXt [55]. The simulations are achieved on MATLAB 2021*a* using core *i*7 3.44 GHz, 16GB RAM, and 4GB graphics card.

TABLE 4. Characteristics of COVID-19 radiography database.

Type	Number of images
COVID-19 (+)	3616
Healthy subjects	10192
Lung opacity	6012
Viral pneumonia	1345

A. DATASET

In this paper, COVID-19 radiography database [56] is used. The main characteristics of the database is presented in Table 4. Since the database is completely imbalanced in nature, therefore, data augmentation is utilized to balance the database. The data augmentation is achieved by considering random blurring, random cropping, and random rotation. Thus, it is used to increase the minority class CXR images for improving the strength of COVID-19 screening model and overcome the overfitting issue. Table 5 depicts the data augmentation approaches used along with their respective parameter settings. Figure 5 shows the sample view of the obtained CXRs from data augmentation approach. Also, all the images are resized to 224 × 224 resolution.

Table 6 shows number of images used for training, validation and testing of the proposed and competitive models. Training fraction also includes augmented images.

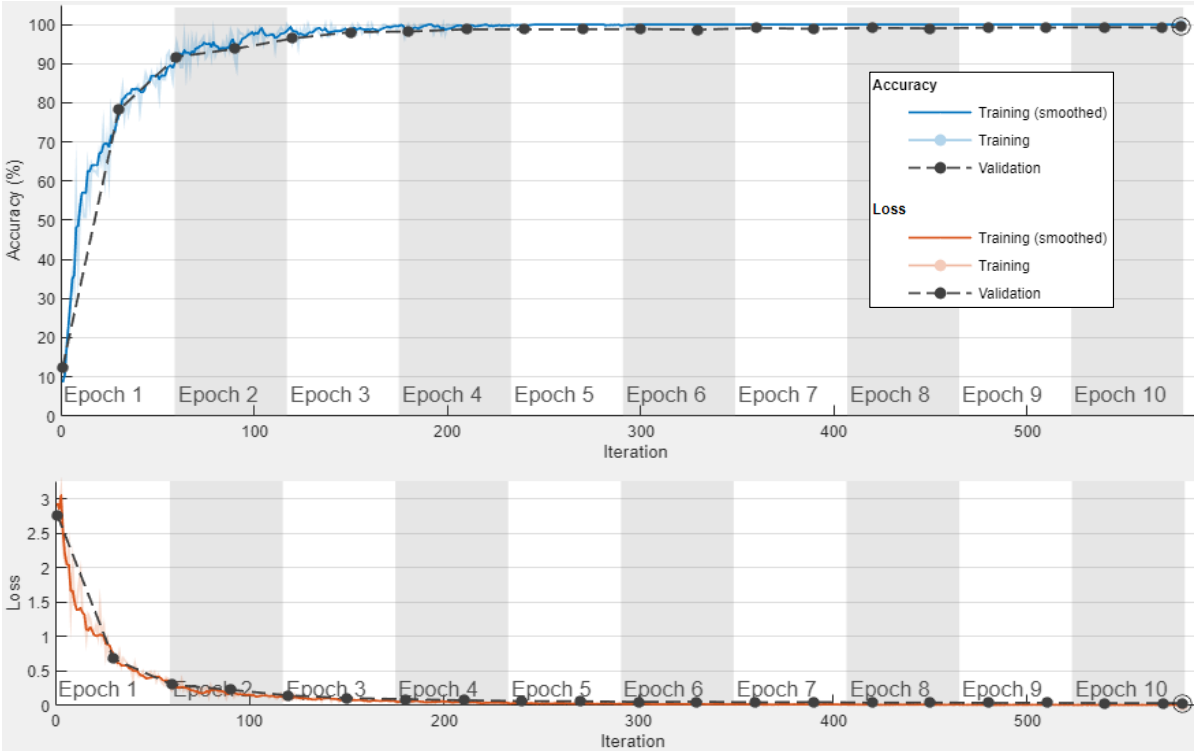

FIGURE 4. Training and validation analysis of MMCGA based proposed model.

TABLE 5. Parameter settings for data augmentation approach.

Approach	Parameter settings
Random Rotate	0^o to 180^o
Random Crop	0 to 25% from every side
Random Blur	Gaussian blur with standard deviation from 0 to 10

TABLE 6. Number of images used for training, validation and testing of proposed model.

Class	Training	Validation	Testing
COVID-19 (+)	10258	361	904
Healthy subjects	14057	1019	2548
Lung opacity	11240	601	1503
Viral pneumonia	9487	134	336

B. PERFORMANCE ANALYSIS

The median and uncertainty values (i.e., median $\pm$ $IQR \times 1.5$) are utilized to evaluate the performance of MMCGA based DCov-Net. 65% of dataset is utilized for building the model. 10% of dataset is utilized for validation of proposed model. 25% of dataset is utilized for testing MMCGA based DCov-Net. The confusion matrix-based performance metrics such as accuracy, specificity, sensitivity, area under curve (AUC) and F-measure are utilized for evaluating the performance of MMCGA based DCov-Net.

AUC - receiver operating characteristic (ROC) curve is a well-known measure for classification problems at different threshold settings. AUC represents a measure of separability and ROC defines a probability curve. AUC-ROC evaluates the performance of the model in terms of differentiating between classes. Maximum AUC values define that the model can efficiently differentiate between positive and

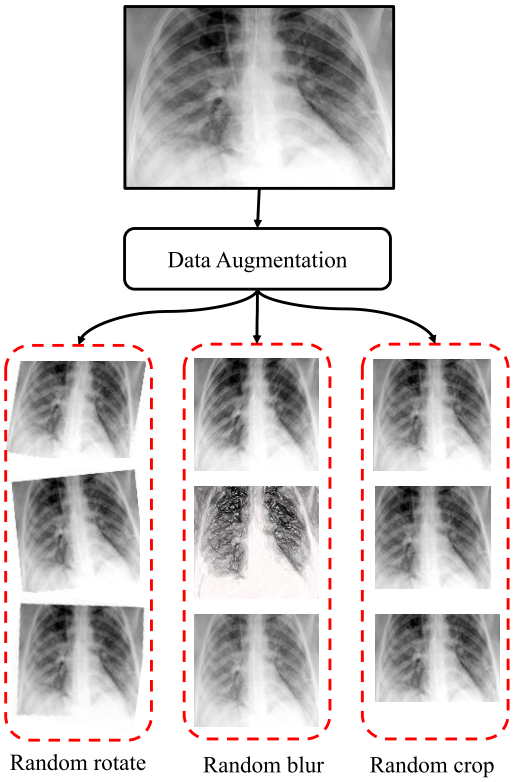

FIGURE 5. Sample view of obtained results from the data augmentation approach.

TABLE 7. Training analysis of MMCGA based DCov-Net-based automatic COVID-19 screening model on four class CXR datasets.

Model	Accuracy	F-measure	Sensitivity	Specificity	AUC
CNN	96.24 ± 1.72	95.57 ± 1.47	95.78 ± 1.26	96.49 ± 1.51	95.92 ± 1.54
Resnet	98.54 ± 1.31	98.25 ± 1.37	98.15 ± 1.43	98.27 ± 1.46	98.13 ± 1.15
VGGnet	97.23 ± 1.15	97.39 ± 1.61	96.94 ± 1.22	98.07 ± 0.97	97.01 ± 0.99
Inceptionnet-v1	98.32 ± 0.95	98.21 ± 0.99	98.12 ± 0.84	98.65 ± 0.93	98.19 ± 1.01
Alexnet	97.83 ± 1.55	97.42 ± 1.25	96.69 ± 1.65	97.83 ± 1.15	97.28 ± 1.13
DenseNet	98.49 ± 0.95	98.43 ± 0.91	98.32 ± 0.89	98.34 ± 0.86	98.35 ± 0.83
Xception	98.52 ± 1.21	98.29 ± 1.41	98.34 ± 1.08	98.42 ± 0.94	98.41 ± 0.91
Inception-Resnet	98.72 ± 1.01	98.76 ± 0.91	98.73 ± 0.85	98.96 ± 0.87	98.96 ± 0.76
Inceptionnet-v3	98.72 ± 1.11	98.67 ± 1.02	98.71 ± 0.87	98.74 ± 1.06	98.77 ± 1.07
ResNeXt	98.81 ± 0.67	98.94 ± 0.68	98.72 ± 0.91	98.83 ± 0.79	98.94 ± 0.71
Inceptionnet-V4	98.53 ± 0.97	98.52 ± 0.79	98.68 ± 0.81	98.86 ± 0.94	98.92 ± 0.74
Proposed MMCGA based DCov-Net	**99.81 ± 0.19**	**99.79 ± 0.20**	**99.75 ± 0.24**	**99.67 ± 0.33**	**99.72 ± 0.28**

TABLE 8. Testing analysis of MMCGA based DCov-Net-based automatic COVID-19 screening model on four class CXR datasets.

Model	Accuracy	F-measure	Sensitivity	Specificity	AUC
CNN	93.88 ± 2.01	93.74 ± 1.84	93.83 ± 1.95	93.66 ± 1.94	93.81 ± 1.91
Resnet	95.71 ± 1.51	95.63 ± 1.55	95.68 ± 1.73	95.61 ± 1.41	95.73 ± 1.45
Inceptionnet-v1	95.91 ± 1.43	95.88 ± 1.39	95.84 ± 1.41	95.83 ± 1.33	95.74 ± 1.33
VGGnet	96.39 ± 1.31	96.19 ± 1.31	95.93 ± 1.31	96.41 ± 1.48	95.23 ± 1.44
Alexnet	96.26 ± 1.81	96.18 ± 1.83	95.91 ± 1.59	96.94 ± 1.33	95.12 ± 1.51
DenseNet	97.51 ± 1.19	97.15 ± 1.13	98.12 ± 1.33	97.25 ± 1.35	97.21 ± 1.24
Xception	97.41 ± 1.09	97.26 ± 1.13	97.33 ± 1.15	97.46 ± 1.09	97.35 ± 1.15
Inception-Resnet	97.31 ± 1.18	97.26 ± 1.28	97.41 ± 0.99	97.49 ± 0.91	97.26 ± 0.94
Inceptionnet-v3	96.21 ± 1.42	96.14 ± 1.44	95.93 ± 1.44	98.04 ± 1.44	96.14 ± 1.37
ResNeXt	98.03 ± 0.91	97.93 ± 0.93	98.47 ± 1.07	97.14 ± 1.01	97.91 ± 1.14
Inceptionnet-V4	97.95 ± 1.12	97.87 ± 1.21	97.54 ± 1.24	98.23 ± 0.95	97.53 ± 0.87
Proposed MMCGA based DCov-Net	**99.34 ± 0.51**	**99.32 ± 0.39**	**99.12 ± 0.38**	**99.34 ± 0.45**	**99.28 ± 0.36**

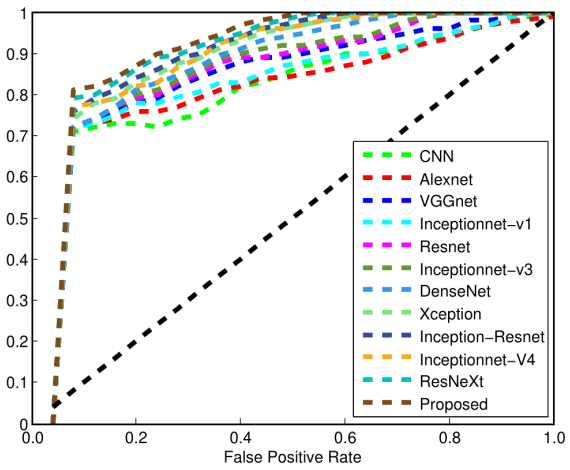

FIGURE 6. Receiver operating characteristic (ROC) curve analysis of the proposed MMCGA based DCoV-Net.

ANOVA Table

Source	SS	df	MS	F	Prob>F
Columns	175.705	11	15.9732	81.73	3.95952e-47
Error	21.108	108	0.1954		
Total	196.814	119			

FIGURE 7. ANOVA analysis of the proposed MMCGA based DCoV-Net in terms of accuracy.

negative classes. ROC curve is drawn with a true positive rate (TPR) against the false positive rate (FPR). It shows specificity and sensitivity analysis for every possible cut-off for a test or a combination of tests. Figure 6 demonstrates that the proposed MMCGA based DCov-Net achieves better AUC values as compared to the existing models. Therefore, the proposed MMCGA based DCov-Net can provide significantly better performance for the initial screening of COVID-19 suspected subjects.

Tables 7 and 8 demonstrates the performance analysis of MMCGA based DCov-Net for COVID-19 suspected subjects. During the training and testing process, MMCGA based DCov-Net achieves the accuracy values 99.81 and 99.34, respectively. Therefore, MMCGA based DCov-Net does not suffer from the overfitting issue. Additionally, during training and testing processing, MMCGA based DCov-Net achieves and AUC values of 99.72 and 99.28, respectively. Therefore, the proposed model is least affected by the false positive and false negative values.

In this paper, a one-way analysis of variance (ANOVA) and boxplot based statistical analysis is also performed by considering the performance of testing results. For every performance metric, the hypotheses can be defined as:

$$\begin{cases} H_0 & \mu M_1 = \mu M_2 = \ldots. = \mu M_{12}, \\ H_A & \text{Means are not equal.} \end{cases} \tag{18}$$

Here, μM_i represents various COVID-19 screening models under consideration. M_{12} represents the proposed model. H_0 and H_A denote null and alternate hypothesis, respectively. From Figures 7 to 15, it is observed that H_A is accepted as all computed $p - values$ are lesser than 0.01. Therefore, there is statistically significant difference in the average performance

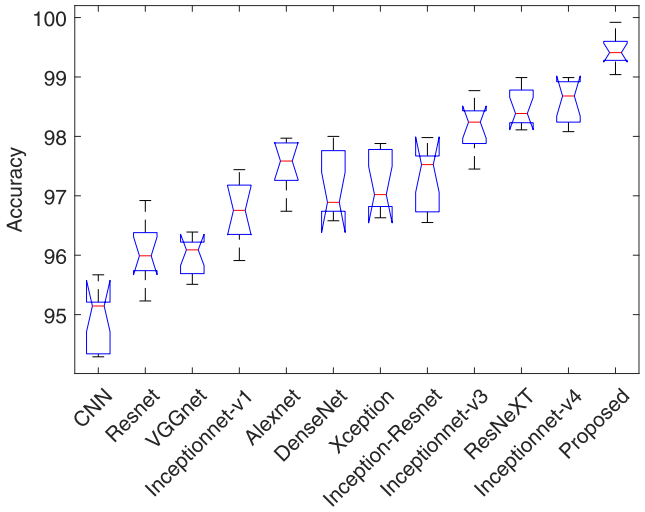

FIGURE 8. Boxplot analysis of the proposed MMCGA based DCoV-Net in terms of accuracy.

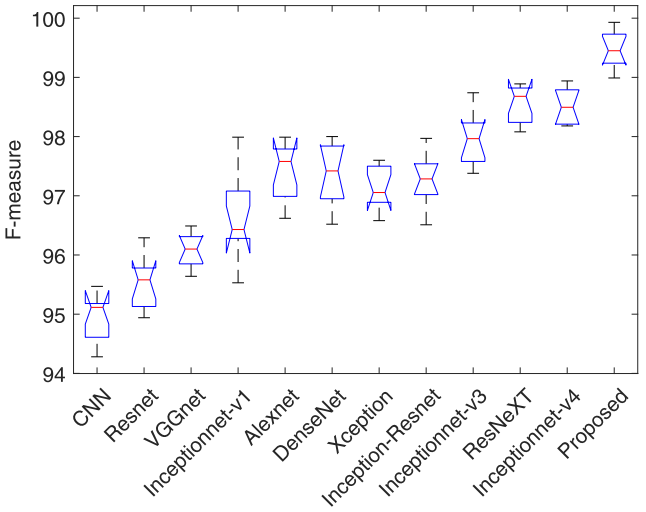

FIGURE 10. Boxplot analysis of the proposed MMCGA based DCoV-Net in terms of f-measure.

ANOVA Table

Source	SS	df	MS	F	Prob>F
Columns	185.902	11	16.9002	88.38	9.28939e-49
Error	20.652	108	0.1912		
Total	206.555	119			

FIGURE 9. ANOVA analysis of the proposed MMCGA based DCoV-Net in terms of f-measure.

ANOVA Table

Source	SS	df	MS	F	Prob>F
Columns	177.85	11	16.1682	80.96	6.21615e-47
Error	21.569	108	0.1997		
Total	199.419	119			

FIGURE 11. ANOVA analysis of the proposed MMCGA based DCoV-Net in terms of sensitivity.

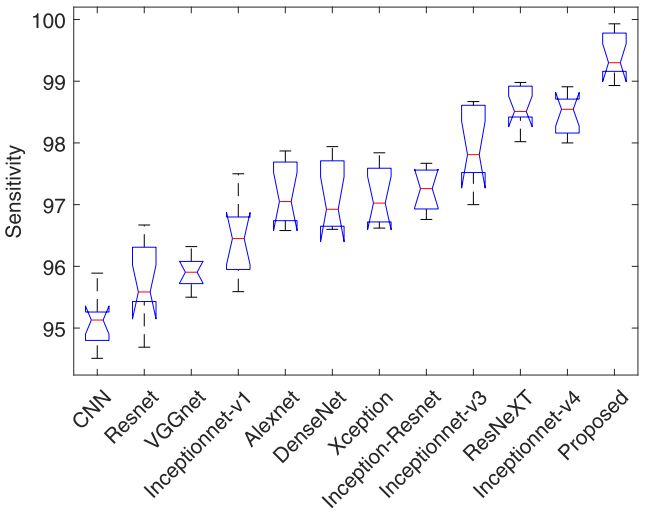

FIGURE 12. Boxplot analysis of the proposed MMCGA based DCoV-Net in terms of sensitivity.

metric values. However, it does not show which of the specific models outperforms others. Therefore, boxplot analysis is performed to check which model perform consistently better than the others (see Figures 8 to 16. Figures 7 - 8 show ANOVA and boxplot analysis of computed accuracy values using the testing data, respectively. It is clearly found that the testing accuracy values obtained from the proposed model are significantly better than the existing models.

Figures 9 and 10 demonstrate ANOVA and boxplot analysis of computed f-measure values using the testing data. It is observed that the f-measure values obtained from MMCGA based DCoV-Net are significantly better than the existing models.

Figures 11 and 12 show ANOVA and boxplot analysis of computed testing sensitivity values. It is clearly found that the sensitivity values obtained from the proposed model are significantly better than the existing models.

Figures 13 and 14 demonstrate ANOVA and boxplot analysis of computed specificity values using the testing data. It is observed that the specificity values obtained from MMCGA based DCoV-Net are significantly better than the existing models.

Figures 15 and 16 show ANOVA and boxplot analysis of computed testing AUC values. It is clearly found that the AUC values obtained from MMCGA based DCoV-Net are significantly better than the existing models.

Majority of the existing models are not interpretable as they do not provide any transparency to the users. Therefore, the concept of heat-maps is used to achieve explainability and interpretability. Heat-maps allow us to understand how the proposed model achieves classification. The objective is to indicate the critical regions in CXRs so that we can understand that whether the proposed model has correctly

ANOVA Table

Source	SS	df	MS	F	Prob>F
Columns	168.097	11	15.2816	84.85	6.57786e-48
Error	19.451	108	0.1801		
Total	187.548	119			

FIGURE 13. ANOVA analysis of the proposed MMCGA based DCoV-Net in terms of specificity.

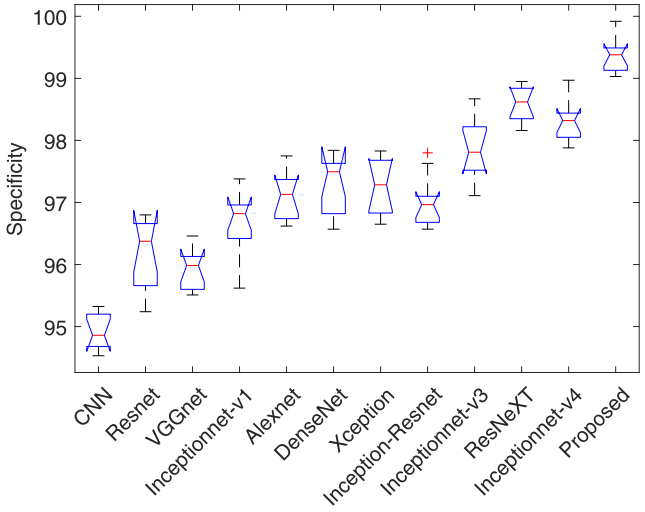

FIGURE 14. Boxplot analysis of the proposed MMCGA based DCoV-Net in terms of specificity.

ANOVA Table

Source	SS	df	MS	F	Prob>F
Columns	204.634	11	18.6031	107.16	7.90634e-53
Error	18.749	108	0.1736		
Total	223.383	119			

FIGURE 15. ANOVA analysis of the proposed MMCGA based DCoV-Net in terms of AUC.

classified the image or not. Figure 17 shows the heat-maps obtained using the proposed model. It is found that there are many dissimilarities between the heat-maps obtained from different class of patients and healthy subjects.

C. DISCUSSION

From the existing literature, it has been found that CXRs can be successfully used for the screening of COVID-19 infected subjects. Many models have been designed and implemented to predict COVID-19 infection in suspected subjects from their respective CXRs. Some well-known COVID-19 automated screening models are DCNN [24], CovXNet [23], Xception [22], MobileNet and SqueezeNet based SVM [25], ChestNet [26], EfficentNet-B0 [27], Hybridized the Xception and ResNet50V2 [28], COVIDiagnosis-Net [29], ResExLBP-SVM [30], CNN-SVM [31], COVIDX-Net [32], COVID-Net [33], CSEN [34]. Although these models have

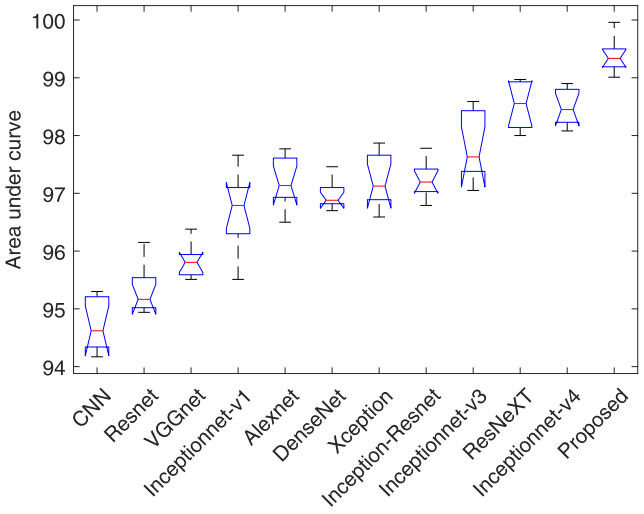

FIGURE 16. Boxplot analysis of the proposed MMCGA based DCoV-Net in terms of AUC.

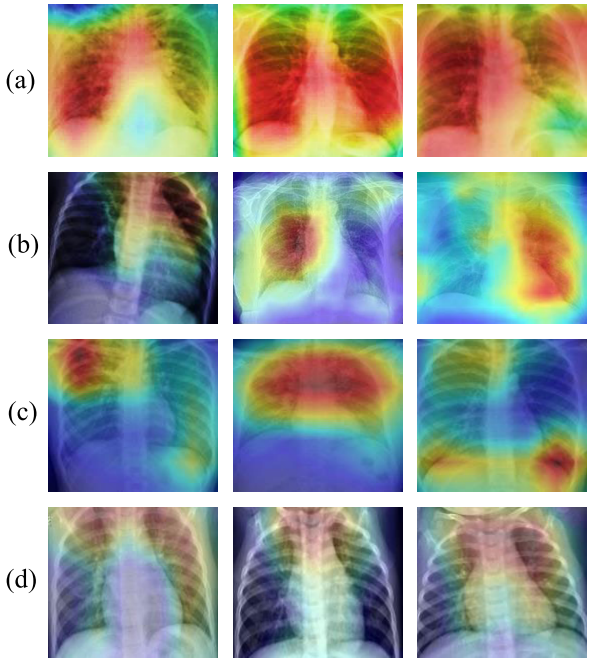

FIGURE 17. Heatmap analysis of the proposed MMCGA based DCov-Net: (a) COVID-19 (+), (b) Pneumonia, (c) Lung opacity, and (d) Healthy subjects.

shown significant results, but the majority of these models have shown poor sensitivity than RT-PCR. Therefore, a fast and efficient COVID-19 automated screening model is proposed for CXR images. Table 9 demonstrates the accuracy analysis among MMCGA based DCov-Net and the existing models. It is found that MMCGA based DCov-Net performs significantly better than the competitive models. DCov-Net is tested on a four-class dataset. Moreover, the sensitivity of MMCGA based DCov-Net approaches towards 100 %. Therefore, the proposed MMCGA based DCov-Net is more reliable for diagnosis of COVID-19 suspected subjects.

TABLE 9. Accuracy analysis among the proposed MMCGA based DCov-Net and state-of-the-art COVID-19 screening models.

Model	Accuracy
DCNN [24]	94.48%
CovXNet [23]	97.40%
Xception [22]	97.41%
MobileNet and SqueezeNet-based SVM [25]	98.25%
ChestNet [26]	94.67%
EfficentNet-B0 [27]	99%
Xception and ResNet50V2 [28]	91.40%
COVIDiagnosis-Net [29]	98.30%
ResExLBP-SVM [30]	99.29%.
CNN-SVM [31]	95.20%
COVIDX-Net [32]	90%
COVID-DenseNet [39]	93.71%
MC-ResNet [40]	95.5%
COVID-Net [33]	93.3%
TL-SVM [36]	94.7%
CSEN [34]	95.9
Proposed MMCGA based DCov-Net	**99.34%**

Additionally, the proposed model takes on average 8.94 minutes for building the multiclass COVID-19 screening model. Furthermore, it can test up to 500 images in one minute. Thus, DCov-Net can screen the COVID-19 suspected subjects at a reasonable time.

V. CONCLUSION

In this paper, DCov-Net was designed for screening COVID-19 suspected subjects from CXR images. However, DCoV-Net is sensitive towards the initial control parameters. Therefore, MMCGA is then proposed to tune the hyper-parameters of DCov-Net. Majority of the existing COVID-19 diagnosis models are not interpretable as they do not provide any transparency to the users. Therefore, in this paper, the concept of heat-maps was utilized to achieve explainability and interpretability. MMCGA based DCov-Net was validated on a multiclass dataset that contains four different classes. Experimental results revealed that MMCGA based DCov-Net achieves better results than the existing models. Therefore, MMCGA based DCov-Net has an ability to be implemented in clinical applications for quick and accurate screening of COVID-19 suspected subjects and potentially other coronaviruses in the future.

In near future, the proposed model can be extended by designing an evolving deep transfer learning model. Since in real-time applications, CXRs may suffer from noise and poor visibility issues, therefore, image preprocessing techniques can also be integrated with the proposed model.

REFERENCES

[1] C. Huang *et al.*, "Clinical features of patients infected with 2019 novel coronavirus in Wuhan, China," *Lancet*, vol. 395, no. 10223, pp. 497–506, May 2020.
[2] E. De Wit, N. Van Doremalen, D. Falzarano, and V. J. Munster, "SARS and MERS: Recent insights into emerging coronaviruses," *Nature Rev. Microbiol.*, vol. 14, no. 8, p. 523, 2016.
[3] C. Mattiuzzi and G. Lippi, "Which lessons shall we learn from the 2019 novel coronavirus outbreak?" *Ann. Transl. Med.*, vol. 8, no. 3, p. 48, Feb. 2020.
[4] H. Li, Y. Wang, J. Xu, and B. Cao, "Potential antiviral therapeutics for 2019 novel coronavirus," *Zhonghua Jie He He Hu Xi Za Zhi=Zhonghua Jiehe He Huxi Zazhi=Chin. J. Tuberculosis Respiratory Diseases*, vol. 43, p. E002, Feb. 2020.
[5] B. Hu, L.-P. Zeng, X.-L. Yang, X.-Y. Ge, W. Zhang, B. Li, J.-Z. Xie, X.-R. Shen, Y.-Z. Zhang, N. Wang, D.-S. Luo, X.-S. Zheng, M.-N. Wang, P. Daszak, L.-F. Wang, J. Cui, and Z.-L. Shi, "Discovery of a rich gene pool of bat SARS-related coronaviruses provides new insights into the origin of SARS coronavirus," *PLOS Pathogens*, vol. 13, no. 11, Nov. 2017, Art. no. e1006698.
[6] S. Roy *et al.*, "Deep learning for classification and localization of COVID-19 markers in point-of-care lung ultrasound," *IEEE Trans. Med. Imag.*, vol. 39, no. 8, pp. 2676–2687, Aug. 2020.
[7] T. Ai, Z. Yang, H. Hou, C. Zhan, C. Chen, W. Lv, Q. Tao, Z. Sun, and L. Xia, "Correlation of chest CT and RT-PCR testing for coronavirus disease 2019 (COVID-19) in China: A report of 1014 cases," *Radiology*, vol. 296, no. 2, 2020, Art. no. 200642.
[8] Z. Han, B. Wei, Y. Hong, T. Li, J. Cong, X. Zhu, H. Wei, and W. Zhang, "Accurate screening of COVID-19 using attention-based deep 3D multiple instance learning," *IEEE Trans. Med. Imag.*, vol. 39, no. 8, pp. 2584–2594, Aug. 2020.
[9] Y. Oh, S. Park, and J. C. Ye, "Deep learning COVID-19 features on CXR using limited training data sets," *IEEE Trans. Med. Imag.*, vol. 39, no. 8, pp. 2688–2700, Aug. 2020.
[10] X. Wang, X. Deng, Q. Fu, Q. Zhou, and J. Feng, "A weakly-supervised framework for COVID-19 classification and lesion localization from chest CT," *IEEE Trans. Med. Imag.*, vol. 39, no. 8, pp. 2615–2625, May 2020.
[11] J. Wang, Y. Bao, Y. Wen, H. Lu, H. Luo, Y. Xiang, X. Li, C. Liu, and D. Qian, "Prior-attention residual learning for more discriminative COVID-19 screening in CT images," *IEEE Trans. Med. Imag.*, vol. 39, no. 8, pp. 2572–2583, Aug. 2020.
[12] D. Fan, T. Zhou, G. Ji, Y. Zhou, G. Chen, H. Fu, J. Shen, and L. Shao, "Inf-Net: Automatic COVID-19 lung infection segmentation from CT images," *IEEE Trans. Med. Imag.*, vol. 39, no. 8, pp. 2626–2637, Aug. 2020.
[13] G. Wang, X. Liu, C. Li, Z. Xu, J. Ruan, H. Zhu, T. Meng, K. Li, N. Huang, and S. Zhang, "A noise-robust framework for automatic segmentation of COVID-19 pneumonia lesions from CT images," *IEEE Trans. Med. Imag.*, vol. 39, no. 8, pp. 2653–2663, Aug. 2020.
[14] Y. Fang, H. Zhang, J. Xie, M. Lin, L. Ying, P. Pang, and W. Ji, "Sensitivity of chest CT for COVID-19: Comparison to RT-PCR," *Radiology*, vol. 296, no. 2, 2020, Art. no. 200432.
[15] X. Xie, Z. Zhong, W. Zhao, C. Zheng, F. Wang, and J. Liu, "Chest CT for typical 2019-nCoV pneumonia: Relationship to negative RT-PCR testing," *Radiology*, vol. 296, no. 2, 2020, Art. no. 200343.
[16] M. Kaur, V. Kumar, V. Yadav, D. Singh, N. Kumar, and N. N. Das, "Metaheuristic-based deep COVID-19 screening model from chest X-ray images," *J. Healthcare Eng.*, vol. 2021, pp. 1–9, Mar. 2021.
[17] G. Mohan and M. M. Subashini, "MRI based medical image analysis: Survey on brain tumor grade classification," *Biomed. Signal Process. Control*, vol. 39, pp. 139–161, Jan. 2018.
[18] J. Ker, L. Wang, J. Rao, and T. Lim, "Deep learning applications in medical image analysis," *IEEE Access*, vol. 6, pp. 9375–9389, 2018.
[19] J. Ker, S. P. Singh, Y. Bai, J. Rao, T. Lim, and L. Wang, "Image thresholding improves 3-dimensional convolutional neural network diagnosis of different acute brain hemorrhages on computed tomography scans," *Sensors*, vol. 19, no. 9, p. 2167, May 2019.
[20] D. Singh, V. Kumar, and M. Kaur, "Densely connected convolutional networks-based COVID-19 screening model," *Appl. Intell.*, vol. 51, no. 5, pp. 3044–3051, 2021.
[21] J. Ker, Y. Bai, H. Y. Lee, J. Rao, and L. Wang, "Automated brain histology classification using machine learning," *J. Clin. Neurosci.*, vol. 66, pp. 239–245, Aug. 2019.
[22] N. N. Das, N. Kumar, M. Kaur, V. Kumar, and D. Singh, "Automated deep transfer learning-based approach for detection of COVID-19 infection in chest X-rays," *IRBM*, Jul. 2020, doi: 10.1016/j.irbm.2020.07.001.
[23] T. Mahmud, M. A. Rahman, and S. A. Fattah, "CovXNet: A multi-dilation convolutional neural network for automatic COVID-19 and other pneumonia detection from chest X-ray images with transferable multi-receptive feature optimization," *Comput. Biol. Med.*, vol. 122, Jul. 2020, Art. no. 103869.
[24] D. Singh, V. Kumar, V. Yadav, and M. Kaur, "Deep convolutional neural networks based classification model for COVID-19 infected patients using chest X-ray images," *Int. J. Pattern Recognit. Artif. Intell.*, vol. 35, no. 3, 2021, Art. no. 2151004.

[25] M. Toğaçar, B. Ergen, and Z. Cömert, "COVID-19 detection using deep learning models to exploit social mimic optimization and structured chest X-ray images using fuzzy color and stacking approaches," *Comput. Biol. Med.*, vol. 121, Jun. 2020, Art. no. 103805.

[26] H. Behzadi-Khormouji, H. Rostami, S. Salehi, T. Derakhshande-Rishehri, M. Masoumi, S. Salemi, A. Keshavarz, A. Gholamrezanezhad, M. Assadi, and A. Batouli, "Deep learning, reusable and problem-based architectures for detection of consolidation on chest X-ray images," *Comput. Methods Programs Biomed.*, vol. 185, Mar. 2020, Art. no. 105162.

[27] A. Altan and S. Karasu, "Recognition of COVID-19 disease from X-ray images by hybrid model consisting of 2D curvelet transform, chaotic salp swarm algorithm and deep learning technique," *Chaos, Solitons Fractals*, vol. 140, Nov. 2020, Art. no. 110071.

[28] M. Rahimzadeh and A. Attar, "A modified deep convolutional neural network for detecting COVID-19 and pneumonia from chest X-ray images based on the concatenation of xception and ResNet50V2," *Informat. Med. Unlocked*, vol. 19, Jan. 2020, Art. no. 100360.

[29] F. Ucar and D. Korkmaz, "COVIDiagnosis-Net: Deep Bayes-SqueezeNet based diagnosis of the coronavirus disease 2019 (COVID-19) from X-ray images," *Med. Hypotheses*, vol. 140, Jul. 2020, Art. no. 109761.

[30] T. Tuncer, S. Dogan, and F. Ozyurt, "An automated residual exemplar local binary pattern and iterative ReliefF based COVID-19 detection method using chest X-ray image," *Chemometric Intell. Lab. Syst.*, vol. 203, Aug. 2020, Art. no. 104054.

[31] A. Alqudah, S. Qazan, H. Alquran, I. Qasmieh, and A. Alqudah, "COVID-19 detection from X-ray images using different artificial intelligence hybrid models," *Jordan J. Electr. Eng.*, vol. 6, no. 2, p. 168, 2020.

[32] E. E.-D. Hemdan, M. A. Shouman, and M. E. Karar, "COVIDX-Net: A framework of deep learning classifiers to diagnose COVID-19 in X-ray images," 2020, *arXiv:2003.11055*. [Online]. Available: http://arxiv.org/abs/2003.11055

[33] L. Wang, Z. Q. Lin, and A. Wong, "COVID-Net: A tailored deep convolutional neural network design for detection of COVID-19 cases from chest X-ray images," *Sci. Rep.*, vol. 10, no. 1, pp. 1–12, 2020.

[34] M. Yamaç, M. Ahishali, A. Degerli, S. Kiranyaz, M. E. H. Chowdhury, and M. Gabbouj, "Convolutional sparse support estimator-based COVID-19 recognition from X-ray images," *IEEE Trans. Neural Netw. Learn. Syst.*, vol. 32, no. 5, pp. 1810–1820, May 2021.

[35] A. Abbas, M. M. Abdelsamea, and M. M. Gaber, "4S-DT: Self-supervised super sample decomposition for transfer learning with application to COVID-19 detection," *IEEE Trans. Neural Netw. Learn. Syst.*, vol. 32, no. 7, pp. 2798–2808, Jul. 2021.

[36] A. M. Ismael and A. Şengür, "Deep learning approaches for COVID-19 detection based on chest X-ray images," *Expert Syst. Appl.*, vol. 164, Feb. 2021, Art. no. 114054.

[37] N. I. Hasan, "A hybrid method of COVID-19 patient detection from modified CT-scan/chest-X-ray images combining deep convolutional neural network and two-dimensional empirical mode decomposition," *Comput. Methods Programs Biomed. Update*, vol. 1, Jan. 2021, Art. no. 100022.

[38] N. Hasan, Y. Bao, A. Shawon, and Y. Huang, "DenseNet convolutional neural networks application for predicting COVID-19 using CT image," *Social Netw. Comput. Sci.*, vol. 2, no. 5, pp. 1–11, Sep. 2021.

[39] L. Sarker, M. M. Islam, T. Hannan, and Z. Ahmed, "COVID-DenseNet: A deep learning architecture to detect COVID-19 from chest radiology images," Tech. Rep. 2020050151, 2020.

[40] S. Misra, S. Jeon, S. Lee, R. Managuli, I.-S. Jang, and C. Kim, "Multi-channel transfer learning of chest X-ray images for screening of COVID-19," *Electronics*, vol. 9, no. 9, p. 1388, Aug. 2020.

[41] H.-C. Shin, H. R. Roth, M. Gao, L. Lu, Z. Xu, I. Nogues, J. Yao, D. Mollura, and R. M. Summers, "Deep convolutional neural networks for computer-aided detection: CNN architectures, dataset characteristics and transfer learning," *IEEE Trans. Med. Imag.*, vol. 35, no. 5, pp. 1285–1298, May 2016.

[42] K. He, X. Zhang, S. Ren, and J. Sun, "Deep residual learning for image recognition," in *Proc. IEEE Conf. Comput. Vis. Pattern Recognit. (CVPR)*, Jun. 2016, pp. 770–778.

[43] S. J. Pan and Q. Yang, "A survey on transfer learning," *IEEE Trans. Knowl. Data Eng.*, vol. 22, no. 10, pp. 1345–1359, Oct. 2010.

[44] F. Zhang, Z. Li, B. Zhang, H. Du, B. Wang, and X. Zhang, "Multi-modal deep learning model for auxiliary diagnosis of Alzheimer's disease," *Neurocomputing*, vol. 361, pp. 185–195, Oct. 2019.

[45] Y. Xue, H. Zhu, J. Liang, and A. Słowik, "Adaptive crossover operator based multi-objective binary genetic algorithm for feature selection in classification," *Knowl.-Based Syst.*, vol. 227, Sep. 2021, Art. no. 107218.

[46] M. Premkumar, P. Jangir, R. Sowmya, H. H. Alhelou, A. A. Heidari, and H. Chen, "MOSMA: Multi-objective slime mould algorithm based on elitist non-dominated sorting," *IEEE Access*, vol. 9, pp. 3229–3248, 2021.

[47] K. Deb, A. Pratap, S. Agarwal, and T. Meyarivan, "A fast and elitist multiobjective genetic algorithm: NSGA-II," *IEEE Trans. Evol. Comput.*, vol. 6, no. 2, pp. 182–197, Apr. 2002.

[48] D. Whitley, "An executable model of a simple genetic algorithm," in *Foundations of Genetic Algorithms*, vol. 2. Amsterdam, The Netherlands: Elsevier, 1993, pp. 45–62.

[49] H. Elmaraghy, V. Patel, and I. B. Abdallah, "Scheduling of manufacturing systems under dual-resource constraints using genetic algorithms," *J. Manuf. Syst.*, vol. 19, no. 3, pp. 186–201, 2000.

[50] L. dos Santos Coelho and P. Alotto, "Multiobjective electromagnetic optimization based on a nondominated sorting genetic approach with a chaotic crossover operator," *IEEE Trans. Magn.*, vol. 44, no. 6, pp. 1078–1081, Jun. 2008.

[51] Y. Xue, B. Xue, and M. Zhang, "Self-adaptive particle swarm optimization for large-scale feature selection in classification," *ACM Trans. Knowl. Discovery From Data*, vol. 13, no. 5, pp. 1–27, Oct. 2019.

[52] I. Alnujaim, H. Alali, F. Khan, and Y. Kim, "Hand gesture recognition using input impedance variation of two antennas with transfer learning," *IEEE Sensors J.*, vol. 18, no. 10, pp. 4129–4135, May 2018.

[53] D. Das, K. Santosh, and U. Pal, "Truncated inception net: COVID-19 outbreak screening using chest X-rays," *Phys. Eng. Sci. Med.*, vol. 43, pp. 1–11, Jun. 2020.

[54] K. Pawar, Z. Chen, N. J. Shah, and G. F. Egan, "Suppressing motion artefacts in MRI using an inception-ResNet network with motion simulation augmentation," *NMR Biomed.*, vol. 19, p. e4225, Dec. 2019, doi: 10.1002/nbm.4225.

[55] D. P. Yadav, A. S. Jalal, D. Garlapati, K. Hossain, A. Goyal, and G. Pant, "Deep learning-based ResNeXt model in phycological studies for future," *Algal Res.*, vol. 50, Sep. 2020, Art. no. 102018.

[56] (Aug. 17, 2021). *COVID-19 Radiography Database*. [Online]. Available: https://www.kaggle.com/tawsifurrahman/covid19-radiography-database

DILBAG SINGH (Member, IEEE) received the M.Tech. degree from the Department of Computer Science and Engineering, Guru Nanak Dev University, India, in 2012, and the Ph.D. degree in computer science and engineering from Thapar University, India, in 2019. He was an Assistant Professor with Manipal University Jaipur, India. He is currently working as a Research Professor with the School of Electrical Engineering and Computer Science, Gwangju Institute of Science and Technology, South Korea. He has authored and coauthored more than 50 SCI/SCI indexed journals, including refereed IEEE/ACM/Springer/Elsevier journals. He has also received three patents, three books, and two book chapters, respectively. His research interests include computer vision, medical image processing, machine learning, deep learning, information security, and meta-heuristic techniques. He is also acting as a Lead Guest Editor of *Mathematical Problems in Engineering*, Hindawi (SCI and Scopus Indexed), an Executive Guest Editor of *Current Medical Imaging*, Bentham Science (SCIE and Scopus Indexed), and an Associate editor of *Open Transportation Journal* (Scopus). He is a Reviewer of more than 60 well-reputed journals, such as IEEE, Elsevier, Springer, SPIE, and Taylor and Francis.

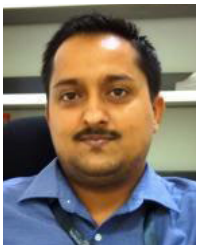

VIJAY KUMAR is currently working as an Assistant Professor with the National Institute of Technology Hamirpur, Hamirpur, India. He has published more than 100 papers in international journals and proceedings of national and international conferences. His research interests include meta-heuristic algorithms, data mining, and pattern recognition.

MANJIT KAUR (Member, IEEE) received the M.E. degree in information technology from Panjab University, Chandigarh, Punjab, India, in 2011, and the Ph.D. degree in the field of image processing from the Thapar Institute of Engineering and Technology, Patiala, Punjab, India, in 2019. She is currently working as an Assistant Professor with the School of Engineering and Applied Sciences, Bennett University, Greater Noida, India. She has published more than 47 SCI/SCIE indexed papers so far. Her research interests include wireless sensor networks, digital image processing, and meta-heuristic techniques.

MOHAMED YASEEN JABARULLA received the B.E. degree in electronics and communications engineering from Anna University, Tamil Nadu, India, in 2011, and the M.S. degree in information and communications and the Ph.D. degree in electrical engineering and computer science from the Gwangju Institute of Science and Technology (GIST), Gwangju, South Korea, in 2016 and 2020, respectively. He is currently working as a Postdoctoral Researcher with the School of Electrical Engineering and Computer Science, GIST, South Korea. His current research interests include computational imaging, machine learning, deep learning, medical image computing, blockchain, eHealth, and biomedical signal processing.

HEUNG-NO LEE (Senior Member, IEEE) received the B.S., M.S., and Ph.D. degrees in electrical engineering from the University of California, Los Angeles, CA, USA, in 1993, 1994, and 1999, respectively. He was with HRL Laboratories, LLC, Malibu, CA, USA, as a Research Staff Member, from 1999 to 2002. From 2002 to 2008, he was an Assistant Professor with the University of Pittsburgh, PA, USA. In 2009, he moved to the School of Electrical Engineering and Computer Science, Gwangju Institute of Science and Technology, Gwangju, South Korea, where he is currently affiliated. His research interests include information theory, signal processing theory, blockchain, communications/networking theory, and their application to wireless communications and networking, compressive sensing, the future Internet, and brain–computer interface. He has received several prestigious national awards, including the top 100 national research and development awards, in 2012, the top 50 achievements of fundamental researches awards, in 2013, and the Science/Engineer of the Month (January 2014).